Journal of Power Sources 264 (2014) 1–7

Contents lists available at ScienceDirect

Journal of Power Sources

journal homepage: www.elsevier.com/locate/jpowsour

Humidity effect on electrochemical performance of Li–O_2 batteries

Ziyang Guo, Xiaoli Dong, Shouyi Yuan, Yonggang Wang*, Yongyao Xia

Department of Chemistry and Shanghai Key Laboratory of Molecular Catalysis and Innovative Materials, Institute of New Energy, Fudan University, Shanghai 200433, China

HIGHLIGHTS

- Humidity is a strong capacity enhancer for the Li–O_2 batteries, but limits the cyclic ability and rate performance.
- Humidity affects the Li_2O_2/O_2 conversion, $LiCO_3/CO_2$ conversion and LiOH formation over charge/discharge cycle.
- Humidity varying results in different morphologies of the discharge products.

ARTICLE INFO

Article history:
Received 26 February 2014
Received in revised form
31 March 2014
Accepted 16 April 2014
Available online 26 April 2014

Keywords:
Li–O_2 battery
Li–air battery
Humidity
O_2 catalytic electrode

ABSTRACT

In this work, we compare the performance of Li–O_2 batteries in pure/dry O_2, pure O_2 with a relative humidity (RH) of 15% and ambient air with an RH of 50%, and analyze the ambient humidity effect on the reactions in the carbon-based catalytic electrode. Electrochemical investigation indicates that discharge capacities of Li–O_2 batteries increased with growth of RH value, but cyclic ability and rate performance are influenced in an opposite way. Ex-situ X-ray diffraction (XRD), Fourier transform-infrared spectrophotometer (FT-IR) and scanning electron microscope (SEM) investigations suggest that ambient humidity affects not only the Li_2O_2/O_2 conversion, $LiCO_3/CO_2$ conversion and LiOH formation but also the morphology of discharge products in porous catalytic electrode over charge/discharge cycle. These results may be important for developing Li–air battery.

1. Introduction

As energy demand is increasing sharply across the world, energy storage will be more crucial in the future than at any time in the past. Among the numerous energy-storage technologies, lithium batteries are important to our daily life. The traditional lithium-ion batteries have been widely used commercially as a power source in the mobile electronics industry because of the highest energy density of all other battery types. Moreover, larger lithium-ion batteries have been used for application in electric vehicles [1,2]. However, the energy density of lithium-ion batteries is now approaching its theoretical limit set by the energies of cathode and anode materials used in these batteries [3]. In recent years, the nonaqueous Li–O_2 batteries have received much attention since they can theoretically store 5–10 times more energy than current Li-ion batteries due to integrating the most electronegative and lightest metal of Li with the extremely electropositive O_2 [4–7]. Furthermore, the cathode active material O_2 is not stored in the battery. Instead, the inexhaustibly oxygen is derived from the ambient environment, which makes the theoretical gravimetric storage capacity of the Li–O_2 batteries far exceed any other battery system known today [8–10]. A typical rechargeable nonaqueous Li–O_2 battery is comprised of a Li-metal anode, a Li conducting organic electrolyte and a porous catalytic cathode [11]. In addition, when in the pure and dry oxygen, the porous electrode reactions on discharge/charge process can be generally summarized as: O_2 enters the porous catalytic cathode and is reduced, then combines with the Li^+ ions in the electrolyte to form solid Li_2O_2 on discharge. Charge reverses the discharge process to release O_2.

Although an apparently simple reaction, several challenges like rechargeability, cycling efficiency, rate capability, electrolyte stability, safety, and charging overpotential still remain to be solved before we can see the practical application of Li–O_2 system on the market [6,12]. So far, extensive efforts have been made to develop a highly effective porous catalytic cathode coupled with a stable electrolyte for high performance rechargeable Li–O_2 batteries, and thus some promising results have been achieved [13–32]. Catalysts like carbon materials [10,16,18,20,28,30], metal nitride [29], noble metals [11,24,26] and transition metal oxides [19,24,31] for rechargeable Li–O_2 battery have been investigated for the above

* Corresponding author. Tel./fax: +86 21 51630318.
E-mail address: ygwang@fudan.edu.cn (Y. Wang).

http://dx.doi.org/10.1016/j.jpowsour.2014.04.079
0378-7753/

goal. In addition, according to recent reports, many commonly used organic carbonate based electrolytes react with the superoxide radical (O_2^-) intermediates produced during the oxygen reduction reaction (ORR) [11,33–37]. For instance, alkyl carbonate was demonstrated to be unstable in the presence of ORR intermediates, which leads to cell failure due to irreversible decomposition at the cathode on discharge to form products such as lithium formate (HCO_2Li), lithium acetate (CH_3CO_2Li), and lithium carbonate (Li_2CO_3), with little or no evidence of the Li_2O_2 formation [11,33–37]. Later work turned to the tetra (ethylene) glycol dimethyl ether and the dimethyl sulfoxide since they are initially promising and certainly more stable to reduced O_2 species than organic carbonates, and they have been studied extensively as Li–O_2 (or air) battery electrolyte solutions [7,8,11,16,18–20,22]. However, it should be noted that these reports mentioned above were generally investigated in pure/dry O_2 atmosphere. It is undoubted that the ultimate target for developing Li–O_2 batteries should be Li–air batteries which can breathe O_2 from environment. Only through this way, Li–O_2 couples could realize the high theoretical energy density that is even compatible with that of gasoline. Therefore, it should be the next logic step for developing Li–air batteries to investigate the ambient humidity effect on the performance of Li–O_2 batteries. However, up to present, this topic is rarely reported.

In present work, carbon (Ketjenblack, KB)-based porous catalytic electrodes were coupled with lithium anodes to form Li–O_2 batteries in tetra(ethylene) glycol dimethyl ether–$LiN(CF_3SO_2)_2$ (TEGDME–LiTFSI) electrolyte. The electrochemical performance of these Li–O_2 batteries in pure/dry O_2 atmosphere, O_2 atmosphere with a relative humidity (RH) of 15% and ambient air atmosphere with an RH of 50% were investigated and compared in detail. Furthermore, Ex-situ XRD, FTIR and SEM technologies were employed to investigate the ambient humidity effect on the reactions in porous catalytic electrode over charge/discharge cycle, including the Li_2O_2/O_2 conversion, Li_2CO_3/CO_2 conversion and LiOH formation.

2. Experimental section

2.1. Preparation of O_2 catalytic electrode

In the preparation of KB-based catalytic O_2 electrode, 80 wt. % KB (Ketjenblack produced by Shanghai Tengmin Industry Co., Ltd, EC600JD; The specific surface area of the KB is 1260 $m^2\ g^{-1}$) and 20 wt. % polyvinylidene fluoride binder (PVDF) were intimately mixed in an *N*-methyl-2-pyrrolidone (NMP) solution, and the resulting slurry was coated on a carbon paper (TGP-H-060 carbon paper, Torray). The total mass loading of KB is 0.8 mg cm^{-2}. The coated electrode was dried for 12 h at 100 °C under vacuum to remove residual solvent.

2.2. Fabrication of Li–O_2 batteries

The batteries assembly was operated in a glove box filled with pure argon. These two electrodes were separated by a separator dipping with TEGDME–(1 M) LiTFSI electrolyte. This Li/separator/O_2 electrode was then sealed into a Swagelok cell with an air hole 0.8 cm^2 placed on the positive electrode side to allow the oxygen to flow in.

2.3. Electrochemical measurements

The cells were cycled in an LAND cycler Wuhan Land Electronic Co. Ltd. Galvanostatic charge–discharge measurements of these Li–O_2 batteries were carried out in a pure/dry oxygen-filled glove box, in an oxygen-filled glove box with the RH of 15 wt. % and in the ambient air with the RH of about 50%, respectively.

2.4. Ex-situ characterization

The ex-situ XRD and FT-IR investigations of porous catalytic electrodes at its pristine state, after full discharge, and after complete recharge were recorded on Bruker D8 Advance Diffractometer using Cu Kα radiation and FI-TR (NICOLET 6700), respectively. The surface morphologies of porous catalytic electrodes at different states were characterized with SEM (FE-SEM S-4800).

3. Results and discussion

3.1. Electrochemical performance of Li–O_2 batteries in pure/dry O_2

Fig. 1a gives the full discharge/charge curves of the Li–O_2 battery in pure/dry O_2 atmosphere with an applied current density of 50 mA g^{-1}. As shown in Fig. 1a, the Li–O_2 cell exhibits rather stable specific capacities above 9500–11,000 mAh g^{-1} for initial 3 cycles. It should be noted that both the applied current density (mA g^{-1}) and the achieved capacity (mAh g^{-1}) were calculated based on the

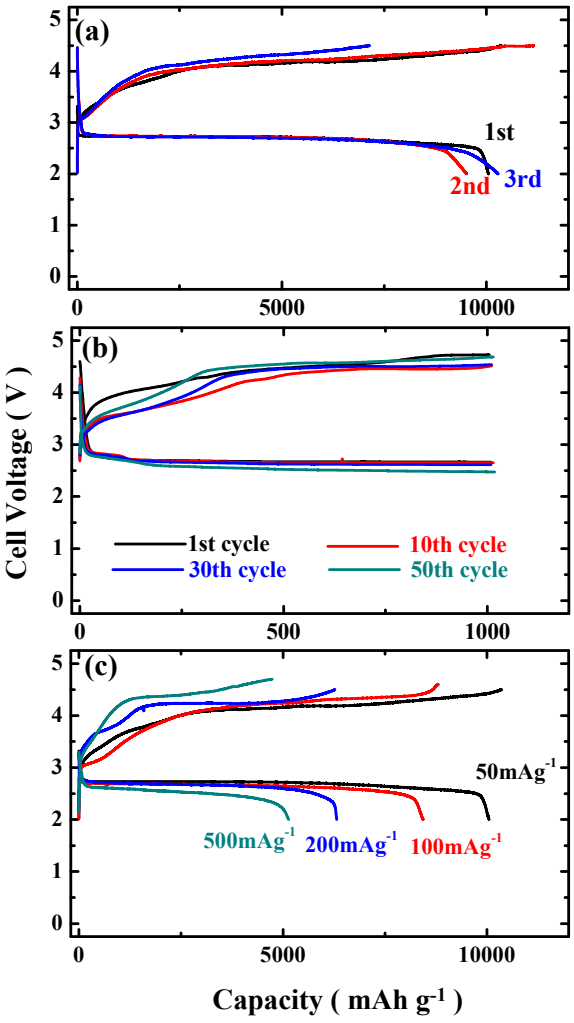

Fig. 1. The discharge/charge curves of Li–O_2 batteries in pure/dry O_2: (a) for initial 3 cycles at a current density of 50 mA g^{-1} with the voltage window of 2 V–4.5 V; (b) at a current density of 200 mA g^{-1} with a fixed capacity of 1000 mAh g^{-1}; (c) at different applied current densities.

carbon mass (KB) in porous catalytic electrode. Moreover, this cell also displays nearly the same discharge voltage platforms for initial 3 cycles. However, the polarization between the discharge and charge slightly increased in the 3rd cycle. The Li–O_2 battery in the 3rd cycle cannot be totally recharged, displaying about 70% of the discharge capacity, which indicates the poor capacity retention after the 3rd cycle. It should be noted that the capacity from the carbon paper (i.e. current collector) is quite limited ($\sim$85 mA g^{-1}) and thus is neglectable, which has been demonstrated by recent reports [14,16].

It should be noted that Li–O_2 batteries generally display poor cyclic performance at full discharge/charge condition, because the high discharge/charge depth may result in more serious volume change (i.e. Li_2O_2/O_2 conversion) and more undesired electrolyte decomposition. Therefore, in a lot of recent investigations [8,14–20,24], Li–O_2 batteries were cycled with a fixed capacity (i.e. limited discharge/charge depth). To further clarify cycle performance of the Li–O_2 batteries in pure/dry O_2, we then tested the Li–O_2 battery cycled at a fixed capacity of 1000 mAh g^{-1} and at a current density of 200 mA g^{-1} (Fig. 1b). As shown in Fig. 1b, the voltage profiles over discharge/charge of the Li–O_2 battery in pure/dry O_2 were reproducible, with no sign of deterioration for initial 30 cycles, which indicates a perfect cycling performance. Even after the 50th cycle, the Li–O_2 battery experienced slight voltage fading.

Fig. 1c shows the discharge/charge curves for the Li–O_2 batteries at different current densities, in pure/dry O_2 atmosphere. It can be detected from Fig. 1c that the polarization between the discharge and charge increased as the applied current densities increased. However, even at the high current density of 500 mA g^{-1}, the Li–O_2 battery still exhibited a stable discharge curve of approximately 2.55 V with a discharge capacity of 5100 mAh g^{-1} that is about 50% of the capacity achieved at the applied current of 50 mA g^{-1}.

3.2. Electrochemical performance of Li–O_2 batteries in O_2 with an RH of 15%

In order to further illustrate the effect of the ambient humidity on the performance of Li–O_2 system, the Li–O_2 batteries were investigated in O_2 atmosphere with an RH of 15%. Fig. 2a shows the discharge/charge profiles of the first 3 cycles for Li–O_2 battery at a current density of 50 mA g^{-1} in O_2 atmosphere with an RH of 15%. As shown in Fig. 2a, the Li–O_2 battery in O_2 atmosphere with an RH of 15 wt. % exhibits a much higher capacity of 18,482 mAh g^{-1} on initial discharge, compared with the initial discharge capacity (10,050 mAh g^{-1}) achieved in pure/dry O_2 atmosphere at the same current density of 50 mA g^{-1}. According to Zhou et al.'s recent report about the operating mechanism of Li–O_2 battery in ambient air [15], the speculated primary reactions of Li–O_2 batteries in O_2 atmosphere with an RH of 15% may be summarized as the following equations:

$$Li^+ + O_2 + e^- \rightarrow LiO_2 \quad (1)$$

$$2LiO_2 \rightarrow Li_2O_2 + O_2 \quad (2)$$

$$2Li_2O_2 + 2H_2O \rightarrow 4LiOH + O_2 \quad (3)$$

As shown in these equations, the discharge of the Li–O_2 battery is initiated with the transient formation of O_2^-, and then reacts with the Li^+ ions to form LiO_2. Next, LiO_2 is decomposed via disproportionation to produce the Li_2O_2 (Reactions (1) and (2)). Obviously, the reaction process of the Li–O_2 battery in pure/dry oxygen just includes reactions (1) and (2). However, when the Li–O_2 cells are operated in O_2 atmosphere with an RH of 15%, some H_2O molecules in ambient condition will also permeate through the oxygen

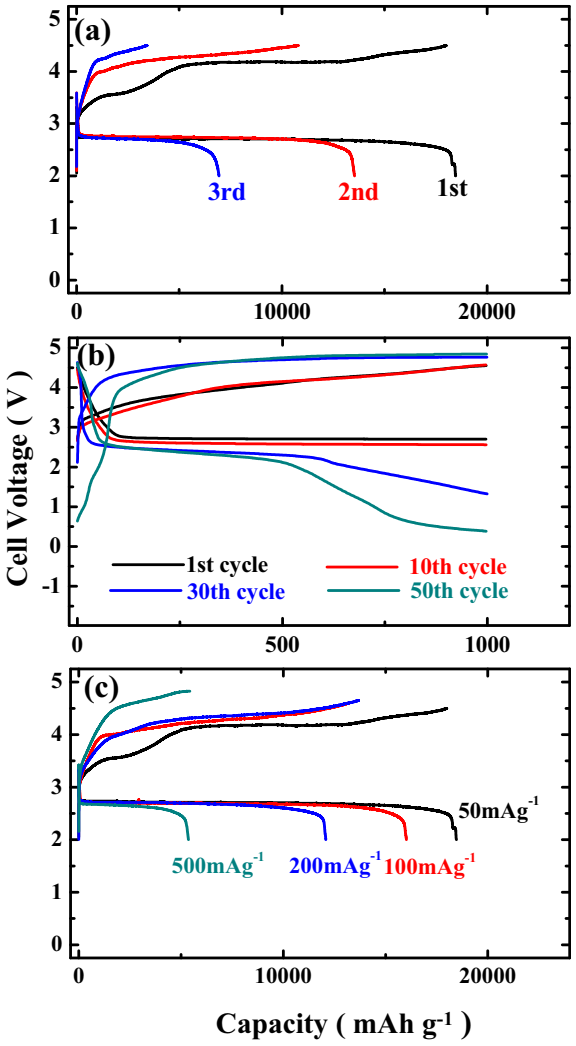

Fig. 2. The discharge/charge curves of Li–O_2 batteries in pure O_2 with an RH of 15%: (a) for initial 3 cycles at a current density of 50 mA g^{-1} with the voltage window of 2 V–4.5 V; (b) at a current density of 200 mA g^{-1} with a fixed capacity of 1000 mAh g^{-1}; (c) at different applied current densities.

channels to react with Li_2O_2 and generate LiOH (Reaction (3)) ultimately. Therefore, due to reaction (3), the Li–O_2 battery in O_2 atmosphere with an RH of 15% displays the much higher first discharge capacity, compared with that in pure/dry O_2 atmosphere. In other words, water was demonstrated to be a strong capacity enhancer for the Li–O_2 battery, which is also consistent with Gasteiger et al.'s recent report [38]. The generation of LiOH over discharge process will be further confirmed by the later ex-situ XRD investigation.

However, the increase of RH much limited the cyclic ability of the Li–O_2 battery. As shown in Fig. 2a, the discharge capacity of the Li–O_2 battery in O_2 atmosphere with an RH of 15% decreased dramatically on cycling down to 6893 mAh g^{-1} after 3 cycles, indicating the poor cycling performance. In addition, we also investigated the cyclic performance of the Li–O_2 battery in O_2 atmosphere with an RH of 15% with a fixed discharge/charge depth. Fig. 2b presents the typical voltage profiles over 50 cycles for the Li–O_2 battery in O_2 atmosphere with an RH of 15% at a fixed capacity of 1000 mAh g^{-1} and at a current density of 200 mA g^{-1}. However, the cycling capability at a fixed capacity of the Li–O_2 battery in O_2 atmosphere with an RH of 15% was greatly

deteriorated, in contrast to that in pure/dry O_2. As shown in Fig. 2b, the Li–O_2 battery in O_2 atmosphere with an RH of 15% experienced voltage fading after the 10th cycle, which also indicates a poor cycling capability. Polarization behavior may arise between the 10th and 50th cycles due to Reaction (3), which results in the irreversible Li_2O_2/O_2 conversion. In addition, RH-induced Li-passivation also contributes to the poor cycle performance.

Fig. 2c presents the discharge/charge profiles for the Li–O_2 batteries at different current densities, in O_2 atmosphere with an RH of 15%. When the current density increases from 50 mA g^{-1} to 500 mA g^{-1}, the discharge capacity of the Li–O_2 batteries in O_2 atmosphere with an RH of 15% gradually decreases from 18,500 mAh g^{-1} to 5348 mAh g^{-1}, indicating the capacity retention of 29%. Obviously, the rate performance (i.e. capacity retention with the increase of applied current densities) of the Li–O_2 battery in O_2 atmosphere with an RH of 15% is much poorer than that in pure/dry O_2 atmosphere. However, it should be noted that at all the current densities of 50 mA g^{-1}, 100 mA g^{-1}, 200 mA g^{-1} and 500 mA g^{-1}, the Li–O_2 batteries in O_2 atmosphere with an RH of 15% exhibit higher discharge capacities than these in pure/dry O_2 atmosphere. As mentioned above, this phenomenon can be also attributed to a certain amount of water, which leads to the formation of LiOH during the discharge process and enhances the discharge capacities (Equations (1)–(3)).

3.3. Electrochemical performance of Li–O_2 batteries in ambient air

In this section, we also investigated the electrochemical performance of Li–O_2 batteries in ambient air with an RH of ~50%. As shown in Fig. 3a, the battery exhibits a single discharge plateau around 2.71 V and a capacity of 9570 mAh g^{-1} in the first cycle with an applied current density of 50 mA g^{-1}. However, the discharge plateau and capacity start to fade immediately after the first cycle. The inferior result should be attributed to the presence of the moisture and CO_2 in the air, which leads to the formation of $LiCO_3$ in porous catalytic cathode and the passivation on Li-anode. As mentioned in above section, a certain amount of water (e.g. RH of 15%) can lead to the formation of LiOH during the discharge process and enhance the discharge capacity. In present case, however, the ~50% RH of ambient air may be too high to ensure the long-time operating of Li–O_2 battery at the low current density of 50 mA g^{-1}. If we increase the applied current density for reducing operating time, the Li–O_2 battery in ambient air atmosphere might display higher discharge capacity. This point will be further discussed in the rate performance investigation.

Next, we further investigated the cyclic performance of the Li–O_2 battery in ambient air atmosphere with a fixed capacity of 1000 mAh g^{-1} at a current density of 200 mA g^{-1}. As shown in Fig. 3b, the Li–O_2 battery experienced dramatic voltage fading after the 10th cycle. Furthermore, the Li–O_2 cell displayed the poor discharge capacity of 300 mAh g^{-1} above the voltage of 0 V, and even was hardly able to be recharged after 10th cycle, exhibiting merely 30% of the discharge capacity below the voltage of 5 V. Obviously, the poor cyclic performance should be ascribed to the air-attacking on porous catalytic electrode and the metallic Li anode.

Fig. 3c shows the first discharge/charge profiles of the Li–O_2 batteries in the air with an RH of ~50 wt. % at current densities of 50, 100, 200, and 500 mA g^{-1}, respectively. Interestingly, it can be seen that, at the current density of 100 mA g^{-1}, the Li–O_2 battery exhibits a much higher discharge capacity of 17,927 mAh g^{-1} than that at the current density of 50 mA g^{-1} (9570 mAh g^{-1}). This phenomenon may occur because both batteries had experienced almost the same attack from the moisture and CO_2 in the air over the same period, which gradually formed the insoluble solid at the

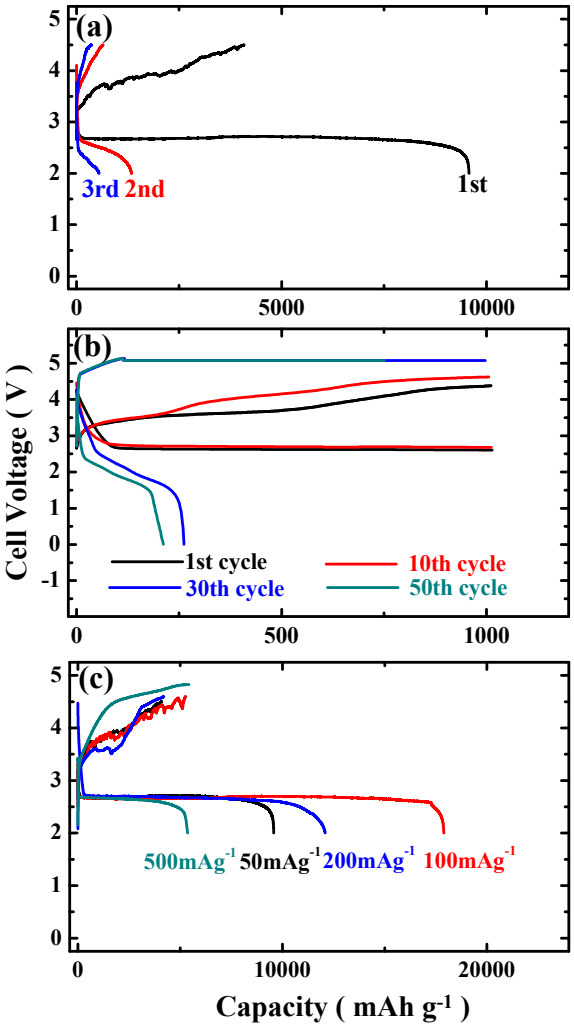

Fig. 3. The discharge/charge curves of Li–O_2 batteries in ambient air with an RH of ~50%: (a) for initial 3 cycles at a current density of 50 mA g^{-1} with the voltage window of 2 V–4.5 V; (b) at a current density of 200 mA g^{-1} with a fixed capacity of 1000 mAh g^{-1}; (c) at different applied current densities.

cathodes blocking the electrolyte and oxygen pathways. While the Li–O_2 battery possessed the lower discharge capacity at the current density of 50 mA g^{-1} compared with that at the current density of 100 mA g^{-1} during the same time. However, the discharge capacity of the Li–O_2 batteries decreased dramatically as the applied current densities continued to increase (above 100 mA g^{-1}). In addition, an unexpected phenomenon happened that the Li–O_2 batteries in the ambient air were unable to be totally recharged, exhibiting under 50% of the discharge capacity when the applied current densities were below 200 mA g^{-1}.

3.4. Ex-situ XRD and FT-IR investigation about these Li–O_2 batteries in different atmospheres

In order to clarify the performance difference of these Li–O_2 batteries operated in various atmospheres, we employed ex-situ XRD and FT-IR technologies to characterize their porous catalytic electrodes at different states. Ex-situ XRD analysis and ex-situ FT-IR analysis were conducted, in sequence, on the Li–O_2 batteries in its pristine state, after full discharge, and after complete recharge.

Fig. 4a gives the XRD patterns at different states of porous catalytic electrodes in Li–O_2 batteries that were operated in the pure/

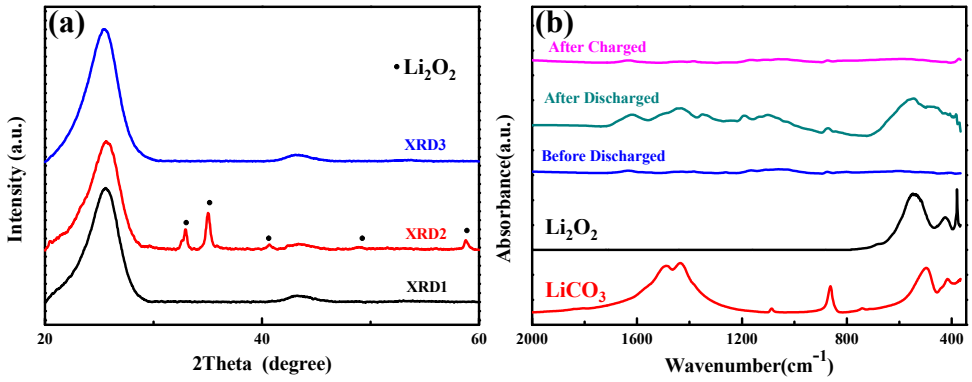

Fig. 4. The analyses for KB electrodes of Li–O_2 batteries in pure/dry O_2: (a) ex-situ XRD patterns at different discharge–charge stages: before discharge (XRD1), after discharge (XRD2) and after recharge (XRD3); (b) ex-situ FTIR spectra before discharge, after discharge and at the end of charge at 1st cycle.

dry O_2 atmosphere. It can be observed from Fig. 4a that the characteristic peaks related to Li_2O_2 exist in the discharge pattern and vanish again in the charge pattern. This was confirmed by the FT-IR spectra data in Fig. 4b, where the characteristic peaks for Li_2O_2, observed at the end of discharge, are absent from the spectrum at the end of charge. The results demonstrate the reversibility of the O_2/Li_2O_2 conversion over the cycles for the Li–O_2 batteries in pure/dry O_2 atmosphere. In the FTIR spectrum of porous catalytic electrode collected at the end of discharge (Fig. 4b), peaks in addition to Li_2O_2 may be assigned to overlap of the bands from HCO_2Li, CH_3CO_2Li, and Li_2CO_3 [27,34,39,40]. The formation of Li carboxylates (i.e. HCO_2Li and CH_3CO_2Li) and Li_2CO_3 should be ascribed to the decomposition of electrolyte on carbon electrode on discharge process [27,34,39,40]. In addition, the decomposition of carbon electrode may also result in the formation of Li_2CO_3 [27,34,39,40]. According to Bruce et al.'s report [27], there is very little decomposition of the carbon electrode on first discharge; overwhelmingly, the side reactions involve decomposition of the electrolyte. In view the results from ex-situ XRD and ex-situ FTIR, we can conclude that the products at the end of the first discharge are overwhelmingly dominated by Li_2O_2, but there is also evidence of the beginning of TEGDME decomposition. Furthermore, this result also highlights the fact that the XRD alone is insufficient to characterize the products of discharge: Li_2O_2 is observable, but less crystalline compounds cannot be detected. On charging, the characteristic peaks of Li_2O_2 disappear in the FTIR spectrum, indicating the main discharge product (i.e. Li_2O_2) was almost removed. In addition, the peaks associated with Li carboxylates and Li_2CO_3 become unclear. This phenomenon is because that these Li carboxylates and Li_2CO_3 formed on discharge can also be decomposed on charging [15,27,34]. Furthermore, recent reports about Li/CO_2 batteries have also demonstrated the reversibly decomposition of $LiCO_3$ on charging [40,41].

The products of the Li–O_2 batteries in O_2 atmosphere with an RH of 15% formed at the end of discharge and charge were also determined by a combination of ex-situ XRD and ex-situ FTIR (Fig. 5). As shown in Fig. 5a, these peaks assigned to overlap of Li_2O_2 and LiOH present in the discharge XRD pattern, which demonstrated the formation of LiOH during the discharge process. More interesting, on recharging, both the Li_2O_2 peaks and LiOH peaks have almost disappeared, which confirmed Zhou et al.'s recent report [15] that LiOH can be decomposed in the recharge of Li–O_2 battery which was operated in ambient air atmosphere. However, as mentioned above, the XRD patterns are not enough to determine the discharge products. Therefore, further investigation has been obtained from the FTIR analysis in Fig. 5b. There is clear FTIR evidence about the generation of Li carboxylates and Li_2CO_3 at the end of discharge, indicating the undesired decomposition of electrolyte. Even at the end of recharge, these characteristic peaks about Li carboxylates and Li_2CO_3 still can be observed clearly in the FTIR spectrum, suggesting that only part Li carboxylates and Li_2CO_3 can be decomposed on recharging.

Finally, we also used ex-situ XRD and ex-situ FTIR technologies to analyze the discharge and charge products of Li–O_2 battery in ambient air with an RH of ~50%. The ex-situ XRD data suggest that the Li_2O_2, LiOH and Li_2CO_3 formed at the end of discharge (Fig. 6a). This result is different from above investigation (i.e. Figs. 4a and 5a). When the Li–O_2 battery was operated in pure/dry O_2 atmosphere

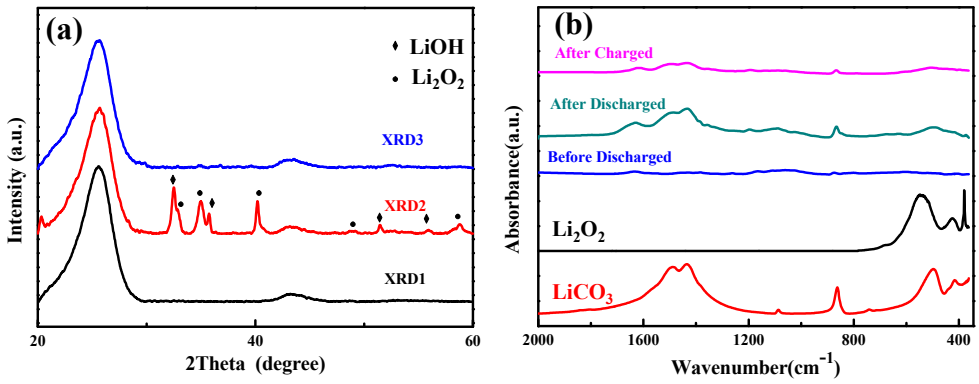

Fig. 5. The analyses for KB electrodes of Li–O_2 batteries in pure O_2 with an RH of 15%: (a) ex-situ XRD patterns at different discharge–charge stages: before discharge (XRD1), after discharge (XRD2) and after recharge (XRD3); (b) ex-situ FTIR spectra before discharge, after discharge and at the end of charge at 1st cycle.

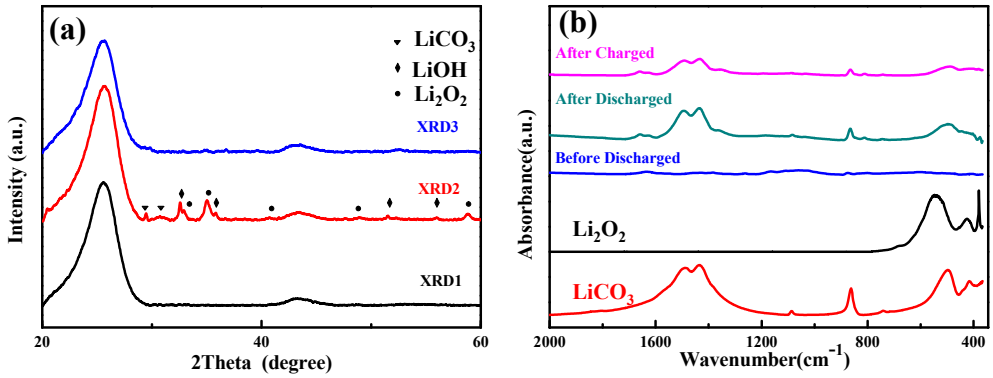

Fig. 6. The analyses for KB electrodes of Li–O_2 batteries in ambient air with an RH of ~50%: (a) ex-situ XRD patterns at different discharge–charge stages: before discharge (XRD1), after discharge (XRD2) and after recharge (XRD3); (b) ex-situ FTIR spectra before discharge, after discharge and at the end of charge at 1st cycle.

or O_2 atmosphere with an RH of 15%, the characteristic peaks corresponding to Li_2CO_3 cannot be observed in the XRD pattern of initial discharge products (see Figs. 4a and 5a). This difference should be ascribed to the CO_2 in ambient air atmosphere. When the Li–O_2 battery was operated in ambient air atmosphere, the Li_2CO_3 could also be formed through direct chemical reactions between CO_2 and LiOH (or Li_2O_2), besides these electrochemical reactions (i.e. electrolyte decomposition and carbon electrode decomposition). These chemical reactions can be summarized as:

$$CO_2 + 2LiOH \rightarrow Li_2CO_3 + H_2O \quad (4)$$

$$CO_2 + Li_2O_2 \rightarrow Li_2CO_3 + \frac{1}{2}O_2\uparrow \quad (5)$$

On the other hand, this result also indicates that the Li_2CO_3 from chemical reactions and the Li_2CO_3 from electrochemical reactions (i.e. electrolyte/electrode decomposition) display different crystalline characteristics. However, the Li_2O_2 peaks were still in presence at the recharge terminal, but the LiOH and $LiCO_3$ peaks have almost disappeared. It suggests that a great deal of the LiOH and $LiCO_3$ were generated upon Li_2O_2 at the terminal stage of discharge, which subsequently mainly recharged but Li_2O_2 remained. It can be assumed that these Li_2O_2 particles were coated by these Li_2CO_3/LiOH particles that generated from the CO_2/H_2O-induced chemical reactions, which limits the oxidation of Li_2O_2 on recharging. Although the ex-situ XRD data at the end of charge suggest that most of the Li_2O_2, LiOH and Li_2CO_3 formed on discharge had been oxidized on charge in Fig. 6a, FTIR again proves more revealing (Fig. 6b). As shown in Fig. 6b, the characteristic peaks corresponding to the Li carboxylates, Li_2CO_3 and Li_2O_2 can be detected in the FTIR spectrum at the end of discharge. However, the characteristic peaks assigned to Li_2CO_3 are obviously clearer than that of Li carboxylates, which is different from above investigation about the Li–O_2 battery in pure/dry O_2 atmosphere or O_2 atmosphere with an RH of 15%. The recharging is a complicated process including the decomposition of the discharge products partially, and the characteristic peaks for Li carboxylates, Li_2CO_3 and Li_2O_2 were still in presence in the FTIR spectrum while the Li_2CO_3 peaks cannot be detected in the XRD pattern on charging due to its less crystalline. According to the results from Fig. 6, we can assume that the crystal Li_2CO_3, which might be produced by the reaction of the Li_2O_2/LiOH and CO_2, can be detected in the XRD pattern and decomposed during the charge process. While the uncrystallized Li_2CO_3, due to the decomposition of the electrolyte or the reaction of Li_2O_2 with carbon (KB), might become the dominant side product and accumulate in the electrode on cycling, in accord with the capacity fading and the poor cycling performance in Fig. 3a and b.

3.5. *Ex-situ SEM about these Li–O_2 batteries in different atmospheres*

Morphologies of the KB-based porous catalytic cathodes at different discharge/charge stages of these Li–O_2 batteries in pure/dry O_2, pure O_2 with an RH of 15% and ambient air with an RH of 50% were systematically investigated by SEM, respectively. Pristine KB-based porous cathodes are shown in Fig. 7a, d and g. It can be seen that they are formed by the aggregation of nanoparticles with typical sizes ranging from 30 to 50 nm in diameter. In addition, a lot of macropores can be observed between KB particles, and these macropores provide a free space for O_2 diffusion and O_2/Li_2O_2 conversion. After discharge, in pure/dry O_2, it can be detected that the morphology of discharge product (Li_2O_2) is the hierarchically porous bird's nest-like structure, which consists of unique nanosheets with <10 nm thicknesses (Fig. 7b). Furthermore, the hierarchically porous bird's nest-like structure of Li_2O_2 vanished after the consequent charge process, indicating the reversible conversion from Li_2O_2 to O_2 as well (Fig. 7c). While in pure O_2 with an RH of 15%, at the end of discharge the surface of the KB-based porous catalytic cathode is almost fully covered by the disc or toroidal particles (Fig. 7e). And the high packing density of the toroid-shaped discharge products may be attributed to the much higher discharge capacity of the Li–O_2 batteries in pure O_2 with an RH of 15%. During the subsequent recharge process, most of the discharge products have been decomposed (Fig. 7f). However, in ambient air with an RH of 50%, the morphology of the discharge products is irregularly spherical solid which consists of a lot of nanosheets (Fig. 7h), compared with the morphology of the discharge product in pure/dry O_2 (Fig. 7b). In addition, after recharge, the irregularly sphere-shaped discharge products are still in presence (Fig. 7i), in consistent with the phenomenon of partially recharged in Fig. 3a.

4. Conclusion

Summarily, ambient humidity effect on the reactions in the carbon-based catalytic electrode of Li–O_2 batteries was investigated in detail. Our results demonstrate that the humidity has an obvious effect on the performance of the Li–O_2 batteries. Specifically, the water can deteriorate cyclic ability and rate ability of the Li–O_2 batteries, while the discharge capacity is enhanced due to the existence of moisture. In addition, the ambient humidity affects not only the Li_2O_2/O_2 conversion, $LiCO_3$/CO_2 conversion and LiOH formation but also the morphology of discharge products in porous catalytic electrode over charge/discharge cycle. Obviously, the effect of the ambient humidity on Li-anode also greatly aggravates

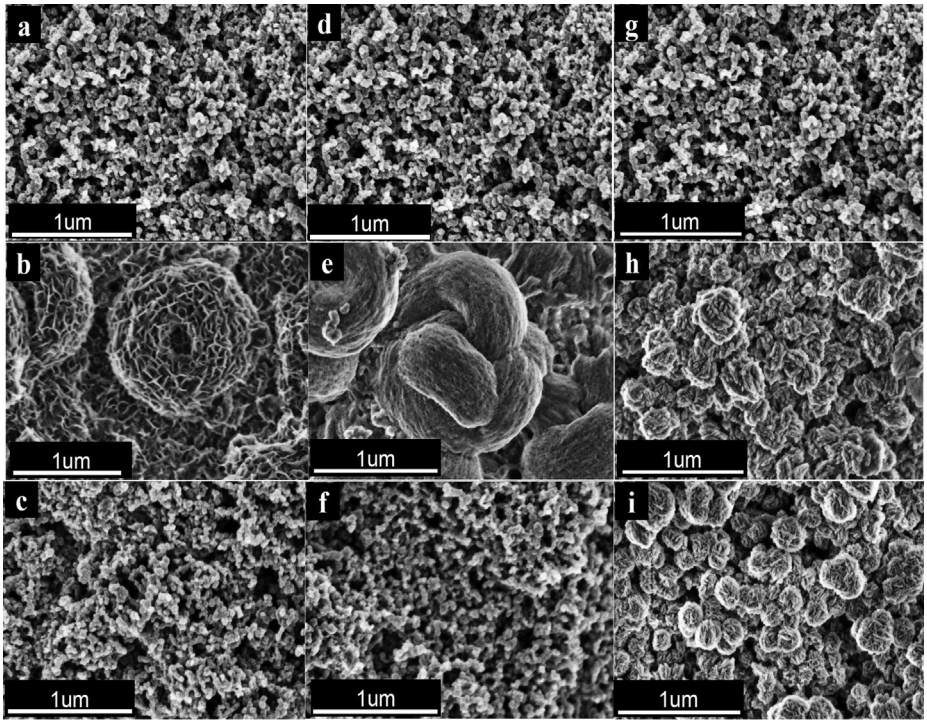

Fig. 7. SEM images of KB electrodes at different states for the Li–O_2 batteries in pure/dry O_2 atmosphere (a, b, c), in O_2 atmosphere with an RH of 15% (d, e, f), and in ambient air with an RH of ~50% (g, h, i): before discharge (a, d, g), after discharge (b, e, h) and after recharge (c, f, i), respectively.

the electrochemical performance difference of these batteries, which should also be investigated in near future.

Acknowledgments

The authors acknowledge funding support from the National Natural Science Foundation of China (21373060, 21103025), Shanghai Pujiang Program (13PJ1400800), and Shanghai Science & Technology Committee (11DZ1100207, 08DZ2270500).

References

[1] T.M. Armand, J.M. Tarascon, Nature 451 (2008) 652–657.
[2] P.G. Bruce, B. Scrosati, J.-M. Tarascon, Angew. Chem. Int. Ed. 47 (2008) 2930–2946.
[3] P.G. Bruce, S.A. Freunberger, L.J. Hardwick, J.-M. Tarascon, Nat. Mater. 11 (2012) 19–29.
[4] K.M. Abraham, Z. Jiang, J. Electrochem. Soc. 143 (1996) 1–5.
[5] T. Ogasawara, A. Debart, M. Holzapfel, P. Novak, P.G. Bruce, J. Am. Chem. Soc. 128 (2006) 1390–1393.
[6] G. Girishkumar, B. McCloskey, A.C. Luntz, S. Swanson, W. Wilcke, J. Phys. Chem. Lett. 1 (2010) 2193–2203.
[7] P.G. Bruce, S.A. Feunberger, L.J. Hardwick, J.M. Tarascon, Nat. Mater. 11 (2013) 19–29.
[8] J.J. Xu, D. Xu, Z.L. Wang, H.G. Wang, L.L. Zhang, X.B. Zhang, Angew. Chem. Int. Ed. 52 (2013) 3887–3890.
[9] S.C. Ma, L.Q. Sun, L.N. Cong, X.G. Gao, C. Yao, X. Guo, L.H. Tai, P. Mei, Y.P. Zeng, H.M. Xie, R.S. Wang, J. Phys. Chem. C 117 (2013) 25890–25897.
[10] J. Xiao, D.H. Mei, X.L. Li, W. Xu, D.Y. Wang, G.L. Graff, W.D. Bennett, Z. Nie, L.V. Saraf, I.A. Aksay, J. Liu, J.G. Zhang, Nano Lett. 11 (2011) 5071–5078.
[11] Z. Peng, S.A. Freunberger, Y.H. Chen, P.G. Bruce, Science 337 (2012) 563–566.
[12] R. Padbury, X. Zhang, J. Power Sources 196 (2011) 4436–4444.
[13] M.M.O. Thotiyl, S.A. Freunberger, Z.Q. Peng, Y.H. Chen, Z. Liu, P.G. Bruce, Nat. Mater. 12 (2013) 1049–1055.
[14] H.G. Jung, J. Hassoun, J.B. Park, Y.K. Sun, B. Scrosati, Nat. Chem. 4 (2012) 579–585.
[15] T. Zhang, H.S. Zhou, Nat. Commun. 4 (2013) 1817, http://dx.doi.org/10.1038/ncomms2855.
[16] J.J. Xu, Z.L. Wang, D. Xu, L.L. Zhang, X.B. Zhang, Nat. Commun. 4 (2013) 2438, http://dx.doi.org/10.1038/ncomms3438.
[17] Z.L. Jian, P. Liu, F.J. Li, P. He, X.W. Guo, M.W. Chen, H.S. Zhou, Angew. Chem. Int. Ed. (2013), http://dx.doi.org/10.1002/anie.201307976.
[18] Z.Y. Guo, D.D. Zhou, X.L. Dong, Z.J. Qiu, Y.G. Wang, Y.Y. Xia, Adv. Mater. 25 (2013) 5668–5672.
[19] Z.L. Wang, D. Xu, J.J. Xu, L.L. Zhang, X.B. Zhang, Adv. Funct. Mater. 22 (2013) 3699–3705.
[20] Z.Y. Guo, J. Wang, F. Wang, D.D. Zhou, Y.Y. Xia, Y.G. Wang, Adv. Funct. Mater. 23 (2013) 4840–4846.
[21] E. Nsybulin, W. Xu, M.H. Englhard, Z.S. Nie, D. Burton, L. Cosimbescu, M.E. Gross, J.G. Zhang, J. Phys. Chem. C 117 (2013) 2635–2645.
[22] H.G. Jung, H.S. Kim, J.B. Park, I.H. Oh, J. Hassoun, C.S. Yoon, B. Scrosati, Y.K. Sun, Nano Lett. 12 (2012) 4333–4335.
[23] C.O. Laoire, S. Mukerjee, E.J. Plichta, M.A. Hendrickson, K.M. Abraham, J. Electrochem. Soc. 3 (2011) A302–A308.
[24] Z.Y. Guo, G.N. Zhu, Z.J. Qiu, Y.G. Wang, Y.Y. Xia, Electrochem. Commun. 25 (2012) 26–29.
[25] Y.C. Lu, Z.C. Xu, H. Gasteiger, S. Chen, K. Hamad-Schifferli, Y. Shao-Horn, J. Am. Chem. Soc. 132 (2010) 12170–12171.
[26] Y.C. Lu, H. Gasteiger, Y. Shao-Horn, J. Am. Chem. Soc. 133 (2011) 19048–19051.
[27] M.M.O. Thotiyl, S.A. Freunberger, Z.Q. Peng, P.G. Bruce, J. Am. Chem. Soc. 135 (2013) 494–500.
[28] R. Black, J.-H. Lee, B. Adams, C.A. Mims, L.F. Nazar, Angew. Chem. Int. Ed. 52 (2013) 392–396.
[29] J.-G. Zhang, D.Y. Wang, W. Xu, J. Xiao, R.E. Williford, J. Power Sources 195 (2010) 4332–4337.
[30] S.Y. Kim, H.-T. Lee, K.-B. Kim, Phys. Chem. Chem. Phys. 15 (2013) 20262–20271.
[31] K. Song, J. Jung, Y.-U. Heo, Y.C. Lee, K. Cho, Y.M. Kang, Phys. Chem. Chem. Phys. 15 (2013) 20075–20079.
[32] S. Meini, N. Tsiouvaras, K.U. Schwenke, M. Piana, H. Beyer, L. Lange, H.A. Gasteiger, Phys. Chem. Chem. Phys. 15 (2013) 11478–11493.
[33] S.A. Freunberger, Y.H. Chen, Z.Q. Peng, J.M. Griffin, L.J. Hardwick, F. Barde, P. Novak, P.G. Bruce, J. Am. Chem. Soc. 133 (2011) 8040–8047.
[34] Y.H. Chen, S.A. Frunberger, Z.Q. Peng, F. Barde, P.G. Bruce, J. Am. Chem. Soc. 134 (2012) 7952–7957.
[35] B.D. McCloskey, D.S. Bethune, R.M. Shelby, G. Girishkumar, A.C. Luntz, J. Phys. Chem. Lett. 2 (2011) 1161–1166.
[36] G.M. Veith, N.J. Dudney, J. Howe, J. Nanda, J. Phys. Chem. C 115 (2011) 14325–14333.
[37] W. Xu, V.V. Viswanathan, D.Y. Wang, S.A. Towne, J. Xiao, Z.M. Nie, D.H. Hu, J.-G. Zhang, J. Power Sources 196 (2011) 3894–3899.
[38] S. Meini, M. Piana, N. Tsiouvaras, A. Garsuch, H.A. Gasteiger, Electrochem. Solid-State Lett. 15 (2012) A45–A48.
[39] B.D. McCloskey, A. Speidel, R. Scheffler, D.C. Miller, V. Viswanathan, J.S. Hummelshøj, J.K. Nørskov, A.C. Luntz, J. Phys. Chem. Lett. 3 (2012) 997–1001.
[40] S.R. Gowda, A. Brunet, G.M. Wallraff, B.D. McCloskey, J. Phys. Chem. Lett. 4 (2013) 276–279.
[41] H.-D. Lim, K.-Y. Park, D.-H. Seo, H. Gwon, J. Hong, William A. Goddard, H. Kim, K. Kang, J. Am. Chem. Soc. 135 (2013) 9733–9742.